Chinese Physics Letters **39**, 123402 (2022)

# Quantum Engineering of Helical Charge Migration in HCCI

ChunMei Liu(刘春梅)[1], Jörn Manz(源满)[2,3,4*], Huihui Wang(王慧慧)[3,4], and Yonggang Yang(杨勇刚)[3,4*]

[1]*Crystal Physics Research Center, College of Science, Nanjing University of Posts and Telecommunications, Nanjing 210023, China*
[2]*Institut für Chemie und Biochemie, Freie Universität Berlin, 14195 Berlin, Germany*
[3]*State Key Laboratory of Quantum Optics and Quantum Optics Devices, Institute of Laser Spectroscopy, Shanxi University, Taiyuan 030006, China*
[4]*Collaborative Innovation Center of Extreme Optics, Shanxi University, Taiyuan 030006, China*

(Received 11 October 2022; accepted manuscript online 8 November 2022)

Electronic charge of molecules can move on time scales when the nuclei stand practically still, from few hundreds of attoseconds to few femtoseconds. This ultrafast process is called "charge migration". A typical consequence is rapid change of electronic dipole, which points to the center of charge. Corresponding linear (one-dimensional, 1D) and planar (2D) dipolar motions have already been well documented. Here we construct the first case of charge migration which causes chiral 3D dipolar motion, specifically along a helix about oriented iodo-acetylene (HCCI). Quantum dynamics simulations show that this can be induced by well-designed laser pulses.

DOI: 10.1088/0256-307X/39/12/123402

Charge migration has been discovered as ultrafast process of electrons, first in linear molecules[1–15] or in quasi-linear ones (e.g., in peptides[16–19]). For example, a laser pulse may photo-ionize the molecule, thus creating an electron hole at one end; the charge will then migrate to the opposite end, on time scale from few hundreds of attoseconds (as) to few femtoseconds (fs). This has, or it may have several consequences: In particular, it induces motions of the electronic dipole (which points to the center of the moving charge) along a line (1D), and we call this "linear charge migration" (LCM). It may also induce sequel processes such as selective bond breaking.[16–18] Subsequently, it was discovered that a laser pulse can also induce circular charge migration (CCM), e.g., about an oriented diatomic molecule[5,20,21] or in a planar molecule (e.g., in benzene[22,23] or in a metal-porphyrin[24–26]). This has consequences which are different from the 1D case of LCM. In particular, CCM induces dipolar motions in a plane (2D).[5,20–39] Moreover, it may generate giant magnetic fields, see, e.g., Refs. [25,26,35,39]. There are also exceptional cases of charge migration which do not change the dipole, cf. Refs. [4,40].

After the familiar 1D and 2D cases of LCM[1–19,28,41] and CCM,[5,20–39] the main purpose of this Letter is to demonstrate, as a proof-of-principle, that charge migration may also induce three-dimensional (3D) motions of the electronic dipole, specifically along a helix about an oriented linear molecule. This will be called "helical charge migration" (HCM). The present HCM should open new applications, e.g., ultrafast manipulation of chirality.

The secondary purpose of this study is to present two different yet equivalent strategies for the design of laser pulses which yield HCM in an oriented linear molecule, and this will be called "quantum engineering of HCM", in analogy to classical engineering of helical motion. The proof of principle will be demonstrated for iodo-acetylene HCCI. This molecule is chosen because it satisfies an important pre-requisite,[42] namely researchers have already demonstrated that it can be oriented along the laboratory $z$-axis, with subsequent ionization and induction of LCM in the cation $HCCI^+$.[8,11,12] Those results stimulated the discovery of decoherence and recoherence of charge migration in $HCCI^+$.[13] The present investigation adapts the scenario of Refs. [8,11,12], i.e., HCCI is oriented along $z$, with the center of mass at the origin and with the nuclei frozen in the global minimum geometry of the electronic ground state. Effects of moving nuclei will be discussed finally. Note, however, that we consider the neutral HCCI (not $HCCI^+$).

Helical motions are coaxial superpositions of linear and circular motions. By analogy, HCM in a linear molecule oriented along $z$ is a coaxial superposition of LCM along $z$ and CCM about the $z$-axis, in brief: HCM = LCM + CCM. This motivates our first strategy for quantum engineering of HCM in the oriented linear molecule. Specifically, we employ a superposition of a linearly $z$-polarized laser pulse and a right circularly polarized laser pulse which propagates in $z$-direction. It is well known that the individual laser pulses induce LCM and CCM. cf., Refs. [1–19,28,41] and Refs. [5,20–39], respectively. As a consequence, the superposition of the two laser pulses should yield the target superposition of charge migration LCM + CCM = HCM.

To demonstrate the quantum engineering of HCM in the oriented HCCI by strategy I (and later on also by strategy II), we shall now present some important properties of the molecule and of the laser pulses. The geometry and the electronic levels of the ground state $1\Sigma^+$ and the degenerate excited states $1\Pi_x, 1\Pi_y$ and $2\Pi_x, 2\Pi_y$ of HCCI oriented along the laboratory $z$-axis are illustrated in Figs. 1(a) and 1(b). The values are listed in the Sup-

*Corresponding authors. Email: ygyang@sxu.edu.cn; jmanz@chemie.fu-berlin.de
© 2022 Chinese Physical Society and IOP Publishing Ltd

porting Information (SI). Linearly $x$-, $y$- and $z$-polarized laser pulses can induce selective symmetry-allowed transitions between these states, as indicated in Fig. 1(b). The corresponding transition matrix elements (TMEs) are also listed in the SI. The levels are the same as those for the set of states $1\Sigma^+$, $1\Pi_+$ and $2\Pi_+$, cf., Fig. 1(c). These states play a key role for our demonstration of the quantum engineering by strategies I and II. For convenience, they are labeled by $j = 0, 1, 2$, respectively. The corresponding levels $E_0 < E_1 < E_2$ and the electronic eigenfunctions $\Psi_0$, $\Psi_1$, and $\Psi_2$ are calculated as solutions of the time-independent electronic Schrödinger equation (TISE) $H_e\Psi_j = E_j\Psi_j$. The corresponding one-electron densities are denoted $\rho_{jj}$. The Hamiltonian $H_e$ accounts for the electronic kinetic energy and for the Coulomb interactions of all electrons and nuclei. The quantum chemical methods for solving the TISE and for calculating the $\rho_{jj}$ and the TME are explained in the SI.

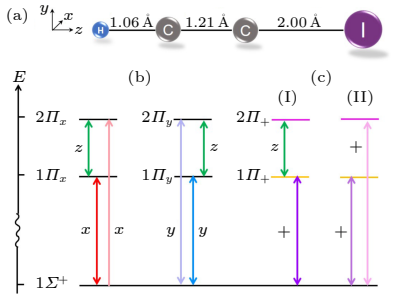


**Fig. 1.** Properties of HCCI oriented along the laboratory $z$-axis. (a) Geometry. (b) Energy levels of the ground state $1\Sigma^+(0.00\,\text{eV})$ and the degenerate excited states $1\Pi_x, 1\Pi_y(5.60\,\text{eV})$ and $2\Pi_x, 2\Pi_y(7.88\,\text{eV})$. Symmetry-allowed resonant transitions between these states can be induced by means of linearly $x$-, $y$- or $z$-polarized laser pulses, as indicated by the vertical double-headed arrows. (c) Same energy levels of states $1\Sigma^+$, $1\Pi_+ = (1\Pi_x + i\cdot 1\Pi_y)/\sqrt{2}$ and $2\Pi_+ = (2\Pi_x + i\cdot 2\Pi_y)/\sqrt{2}$. Strategy I (left) employs a superposition of right (+) circularly and linearly $z-$polarized laser pulses. Strategy II (right) employs right circularly polarized laser pulses, only. The laser pulses induce symmetry-allowed resonant transitions between the states, as indicated by the vertical double-headed arrows.

The laser induced resonant transitions for strategies I and II are indicated in Fig. 1(c). The electric fields of the employed transform limited right (+) circularly and linearly $z$-polarized laser pulses are designed as

$$\begin{aligned}\boldsymbol{\epsilon}_+(t;lp_+) &= \epsilon_x(t;lp_+)\boldsymbol{e_x} + \epsilon_y(t;lp_+)\boldsymbol{e_y}\\ &\equiv \epsilon_+\exp(-t^2/\tau_+^2)\cdot[\cos(\omega_+t+\eta_+)\boldsymbol{e_x}\\ &\quad + \sin(\omega_+t+\eta_+)\boldsymbol{e_y}]\\ \boldsymbol{\epsilon}_{\boldsymbol{z}}(t;lp_z) &= \epsilon_z(t;lp_z)\boldsymbol{e_z} \equiv \epsilon_z\exp(-t^2/\tau_z^2)\cos(\omega_z t+\eta_z)\boldsymbol{e_z}.\end{aligned} \tag{1}$$

The laser parameters $lp = \{\epsilon, \tau, \omega, \eta\}$ include the field strength $\epsilon$, the duration $\tau$, the resonant carrier frequency $\omega$, and the carrier envelope phase (CEP) $\eta$. The unit vectors $\boldsymbol{e_x}, \boldsymbol{e_y}, \boldsymbol{e_z}$ point to the laboratory $x, y, z$ directions. The $lp$'s and the corresponding periods $T = 2\pi/\omega$ are labelled either by subscripts + and $z$ for the polarizations, or by the corresponding target transitions between levels $j$ and $k$, e.g., $\omega_+ = \omega_{01} = (E_1 - E_0)/\hbar$ for the resonant frequency of the transition between states $j = 0$ and 1. Strategies I and II employ superpositions of the laser pulses with total field strengths

$$\begin{aligned}\boldsymbol{\epsilon}_{\text{I}}(t) &= \boldsymbol{\epsilon}_+(t;lp_{01}) + \boldsymbol{\epsilon}_{\boldsymbol{z}}(t;lp_{12}),\\ \boldsymbol{\epsilon}_{\text{II}}(t) &= \boldsymbol{\epsilon}_+(t;lp_{01}) + \boldsymbol{\epsilon}_+(t;lp_{02}).\end{aligned} \tag{2}$$

The values of the $lp$'s are listed in the SI. The laser pulses are negligible and hence they are set equal to zero before the initial time $t_\text{i} = -5\,\text{fs}$ and after the final time $t_\text{f} = 5\,\text{fs}$.

The laser pulses drive the electronic wavefunction from the initial ground state $\Psi(t = t_\text{i}) = \Psi_0$ to the superposition state

$$\Psi(t) = c_0(t)\Psi_0 + c_1(t)\Psi_1 + c_2(t)\Psi_2, \tag{3}$$

with populations $P_j(t) = |c_j(t)|^2$ of the electronic eigenstates $\Psi_j$. The wavefunction (3) is obtained as solution of the time-dependent Schrödinger equation (TDSE) $i\hbar\frac{\partial}{\partial t}\Psi(t) = H(t)\Psi(t)$, with $H(t) = H_\text{e} - \hat{\boldsymbol{d}}\cdot\boldsymbol{\epsilon}(t)$, in semi-classical dipole ($\hat{\boldsymbol{d}}$) approximation. The methods for solving the TDSE and for calculating the coefficients $c_j(t)$ are explained in the SI. The SI also has the method for designing the laser pulses such that they yield arbitrarily chosen target values of the coefficients at the end of the laser pulse, $C_j = c_j(t_\text{f})$. Thereafter, i.e., for times $t' = t - t_\text{f} > 0$, the populations are robust, $P_j(t') = P_j(t_\text{f}) = |C_j|^2$, and the coefficients evolve with time-dependent phases, $c_j(t') = C_j\exp(-iE_jt'/\hbar)$. The wavefunction (3) then represents the laser-induced HCM. Following the examples of Refs. [5,28,43,44], this shall be documented by the time-dependent dipole $\boldsymbol{d}(t')$. The calculations of $\rho(t')$ and $\boldsymbol{d}(t')$ are explained in the SI. Supplementary snapshots of the one-electron density $\rho(t')$ or the difference $\Delta\rho(t') = \rho(t') - \bar{\rho}$ between $\rho(t')$ and its mean $\bar{\rho} = \Sigma_j P_j(t_\text{f})\rho_{jj}$ are also shown in the SI.

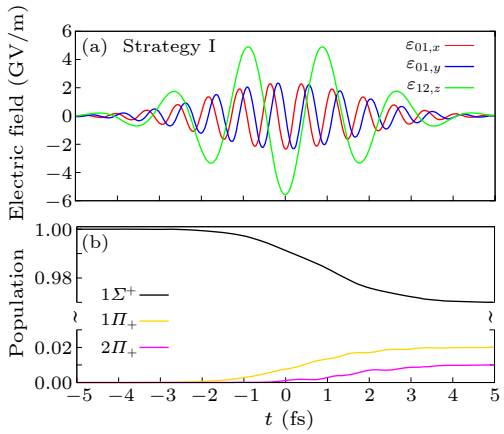


**Fig. 2.** Laser engineering of helical charge migration (HCM) of HCCI oriented along the laboratory $z$-direction by a superposition of right circularly and linearly $z$-polarized laser pulses (Strategy I). (a) Electric field components, cf., Eqs. (1) and (2) with parameters in the SI. (b) The resulting populations $P_j(t)$ of states $1\Sigma^+(j = 0)$, $1\Pi_+(j = 1)$, and $2\Pi_+(j = 2)$. The subsequent HCM is illustrated in Fig. 3 and Fig. SI-1.

The $x$-, $y$-, $z$-components of the electric fields of the superimposed right (+) circularly and linearly $z$-polarized laser pulses for strategy I are illustrated in Fig. 2(a). The $lp$'s are listed in the SI. The resulting populations $P_j(t)$ of

eigenstates $\Psi_j$ are shown in Fig. 2(b). The laser pulses are designed such that at the end, they yield $P_0(t_f) = 0.97$, $P_1(t_f) = 0.02$, $P_2(t_f) = 0.01$, with real-valued coefficients $C_j = c_j(t_f) = \sqrt{P_j}(t_f)$.

As is expected, the superposition of the right circularly and linearly $z$-polarized laser pulses for strategy I yields a superposition of circular plus linear charge migrations, i.e., helical charge migration, in brief, CCM + LCM = HCM. This is also obvious from the time evolution of the dipole $\boldsymbol{d}(t')$.[5,28,43,44] The present strategy I yields the helical path of $\boldsymbol{d}(t')$ shown in Fig. 3. The individual components $d_x(t'), d_y(t')$ and $d_z(t')$ of the chiral $\boldsymbol{d}(t')$ are shown in Fig. SI-2. They confirm the superposition HCM = CCM + LCM.

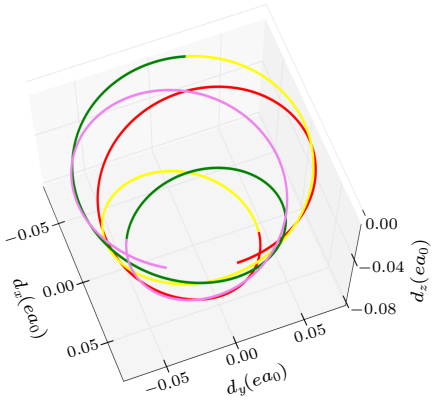


**Fig. 3.** Perspective view of the helical path of the time-dependent dipole $\boldsymbol{d}(t')$, mapping helical charge migration (HCM) in HCCI oriented along $z$ in the laboratory frame, for times $t' = t - t_f > 0$ after the laser pulses for strategies I or II. The sequence of rainbow colors is for the periods $[0, T_{12}/2]$ (red), $[T_{12}/2, T_{12}]$ (yellow), $[T_{12}, 3T_{12}/2]$ (green), and $[3T_{12}/2, 2T_{12}]$ (violet), $T_{12}/2 = 900$ as.

Let us now proceed to the alternative strategy II. It is motivated by classical engineering which substitutes the linear motion of a piston by the rotation of a wheel. By analogy, the present quantum engineering substitutes the linearly polarized laser pulse for the transition from $1\Pi_+(j = 1)$ to $2\Pi_+(j = 2)$ of strategy I by another right circularly polarized laser pulse, for the resonant transition from $1\Sigma^+(j = 0)$ directly to $2\Pi_+(j = 2)$, cf., Fig. 1(c). We keep the right circularly polarized laser pulse of strategy I for resonant transition from the ground state $1\Sigma^+(j = 0)$ to the first excited state $1\Pi_+(j = 1)$, albeit with re-adjusted $lp$'s. The two circularly polarized laser pulses for strategy II are documented in Fig. 4(a). The resulting populations $P_j(t)$'s are in Fig. 4(b). The $lp$'s are in the SI. The laser pulses are designed such that at the end, the populations $P_j(t_f)$ and also the coefficients $c_j(t_f)$ of strategy II are the same as those for strategy I. As a consequence, the subsequent HCM (Fig. 3 and Figs. SI-1 and SI-2) is exactly the same for both strategies I and II.

In conclusion, the results shown in Figs. 2–4 and Fig. SI-1 document equivalent quantum engineering of helical charge migration (HCM) in oriented HCCI, by means of two entirely different strategies. Strategy I is based on considering HCM as superposition of circular plus linear charge migrations, HCM = CCM + LCM. Accordingly, it prepares HCM by means of a superposition of circularly and linearly polarized laser pulses. Strategy II substitutes the linearly polarized laser pulse of strategy I by another circularly polarized pulse. This provides a quantum engineering analogue of the classical substitution of the linear motion of a piston by the rotation of a wheel.

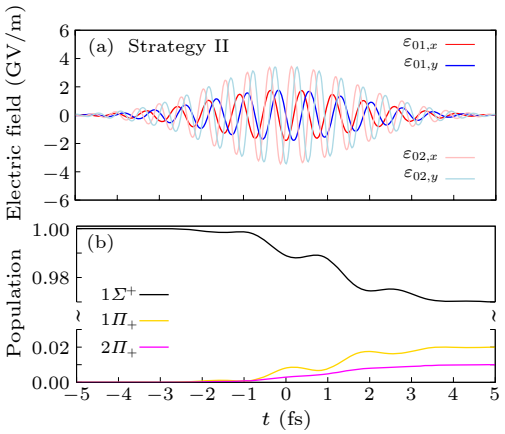


**Fig. 4.** Laser engineering of helical charge migration (HCM) of HCCI oriented along the laboratory $z$-direction by means of two right circularly polarized laser pulses (strategy II). The notations are the same as those for Fig. 2. The subsequent HCM induced by the laser pulses for strategy II is the same as for strategy I, cf., Fig. 3 and Figs. SI-1 and SI-2.

The present proof of the principle should be considered as first step into mostly unexplored territory of research on helical or alternative 3D charge migrations in oriented linear molecules, or in other suitable molecular systems. The field has many challenges: (i) Search for molecules with larger charges which can be driven along helices. (ii) Investigations of the role of nuclear motions and distributions. These tend to induce decoherence of charge migration.[6,43,45] This calls for the search for helical charge migration in systems with long decoherence times. It is encouraging that the literature has prominent examples of charge migrations which last for longer than 10 fs (i.e., for longer than the total duration of the present laser pulses),[22,46] or even with recoherences after tens of femtoseconds.[13] (iii) Monitoring helical charge migrations. Again, it is encouraging that the literature has several methods which could be applied, or developed further for this purpose.[4,47–51] (iv) Exploring the consequences of the transient chirality imposed by helical charge migration. For example, we consider the recent demonstration of time-resolved neighbor roles in the dynamics of molecules in a dimer as stimulating.[52] As analogous working hypothesis, helical charge migration induced in an achiral molecule may effect different dynamics in neighboring molecules with different chiralities. Work along these lines is in progress.

*Acknowledgments.* This work was supported by the National Key Research and Development Program of China (Grant No. 2017YFA0304203), the Program for Changjiang Scholars and Innovative Research Team (Grant No. IRT17R70), the National Natural Science Foundation of China (Grant Nos. 12004193 and 11904215), the 111 Project (Grant No. D18001), the Fund for Shanxi

1331 Project Key Subjects Construction, the Hundred Talent Program of Shanxi Province, and NJUPT-SF (Grant No. NY220089).

# References


[1] Eyring H, Walter J, and Kimball G E 1944 *Quantum Chemistry* (New York: Wiley) chap 11

[2] Cederbaum L S and Zobeley J 1999 *Chem. Phys. Lett.* **307** 205

[3] Breidbach J and Cederbaum L S 2003 *J. Chem. Phys.* **118** 3983

[4] Chelkowski S, Yudin G L, and Bandrauk A D 2006 *J. Phys. B* **39** S409

[5] Nest M, Remacle F, and Levine R D 2008 *New J. Phys.* **10** 025019

[6] Bandrauk A D, Chelkowski S, Corkum P B, Manz J, and Yudin G L 2009 *J. Phys. B* **42** 134001

[7] Kling M F, von den Hoff P, Znakovskaya I, and de Vivie-Riedle R 2013 *Phys. Chem. Chem. Phys.* **15** 9448

[8] Kraus P M, Mignolet B, Baykusheva D *et al.* 2015 *Science* **350** 790

[9] Diestler D, Hermann G, and Manz J 2017 *J. Phys. Chem. A* **121** 5332

[10] Ding H, Jia D, Manz J, and Yang Y 2017 *Mol. Phys.* **115** 1813

[11] Wörner H J, Arrell C A, Banerji N *et al.* 2017 *Struct. Dyn.* **4** 061508

[12] Kraus P M and Wörner H J 2018 *Angew. Chem. Int. Ed.* **57** 5228

[13] Jia D M, Manz J, and Yang Y G 2019 *J. Phys. Chem. Lett.* **10** 4273

[14] Jia D, Manz J, Schild A, Svoboda V, and Yang Y 2020 *From Nuclear Fluxes During Tunnelling to Electronic Fluxes During Charge Migration*, in *Tunnelling in Molecules: Nuclear Quantum Effects from Bio to Physical Chemistry*, edited by Kästner J and Kozuch S, *Theoretical and Computational Chemistry Series No. 18* (London: The Royal Society of Chemistry) chap 5 p 167

[15] Folorunso A S, Bruner A, Mauger F *et al.* 2021 *Phys. Rev. Lett.* **126** 133002

[16] Weinkauf R, Schanen P, Yang D, Soukara S, and Schlag E W 1995 *J. Phys. Chem.* **99** 11255

[17] Remacle F, Levine R D, Schlag E W, and Weinkauf R 1999 *J. Phys. Chem. A* **103** 10149

[18] Kuleff A I, Lünnemann S, and Cederbaum L S 2013 *Chem. Phys.* **414** 100

[19] Kuś T, Mignolet B, Levine R D, and Remacle F 2013 *J. Phys. Chem. A* **117** 10513

[20] Barth I, Manz J, and Serrano-Andrés L 2008 *Chem. Phys.* **347** 263

[21] Yuan K J, Shu C C, Dong D, and Bandrauk A D 2017 *J. Phys. Chem. Lett.* **8** 2229

[22] Mineo H, Lin S H, and Fujimura Y 2014 *Chem. Phys.* **442** 103

[23] Jia D M, Manz J, Paulus B, Pohl V, Tremblay J C, and Yang Y G 2017 *Chem. Phys.* **482** 146

[24] Barth I and Manz J 2006 *Angew. Chem. Int. Ed.* **45** 2962

[25] Barth I, Manz J, Shigeta Y, and Yagi K 2006 *J. Am. Chem. Soc.* **128** 7043

[26] Barth I and Manz J 2010 *Progress in Ultrafast Intense Laser Science VI* (Berlin: Springer) vol 128 p 7043

[27] Kanno M, Kono H, and Fujimura Y 2006 *Angew. Chem. Int. Ed.* **45** 7995

[28] Remacle F, Nest M, and Levine R D 2007 *Phys. Rev. Lett.* **99** 183902

[29] Remacle F, Kienberger R, Krausz F, and Levine R D 2007 *Chem. Phys.* **338** 342

[30] Kanno M, Hoki K, Kono H, and Fujimura Y 2007 *J. Chem. Phys.* **127** 204314

[31] Kanno M, Kono H, Fujimura Y, and Lin S H 2010 *Phys. Rev. Lett.* **104** 108302

[32] Mineo H, Lin S H, and Fujimura Y 2013 *J. Chem. Phys.* **138** 074304

[33] Mineo H, Lin S H, Fujimura Y *et al.* 2013 *J. Chem. Phys.* **139** 214306

[34] Yamaki M, Mineo H, Teranishi Y *et al.* 2014 *J. Phys. Chem. Lett.* **5** 2044

[35] Yuan K J and Bandrauk A D 2015 *Phys. Rev. A* **92** 063401

[36] Yamaki M, Teranishi Y, Nakamura H, Lin S H, and Fujimura Y 2016 *Phys. Chem. Chem. Phys.* **18** 1570

[37] Yamaki M, Mineo H, Teranishi Y, Lin S H, and Fujimura Y 2016 *J. Chin. Chem. Soc.* **63** 87

[38] Mineo H, Yamaki M, Kim G S, Teranishi Y, Lin S H, and Fujimura Y 2016 *Phys. Chem. Chem. Phys.* **18** 26786

[39] Yuan K J, Guo J, and Bandrauk A D 2018 *Phys. Rev. A* **98** 043410

[40] Despré V, Marciniak A, Loriot V *et al.* 2015 *J. Phys. Chem. Lett.* **6** 426

[41] Lünnemann S, Kuleff A I, and Cederbaum L S 2008 *Chem. Phys. Lett.* **450** 232

[42] Ren D, Wang S, Chen C *et al.* 2022 *J. Phys. B* **55** 175101

[43] van den Wildenberg S, Mignolet B, Levine R D, and Remacle F 2019 *J. Chem. Phys.* **151** 134310

[44] Wang H, Jiao Y, Zhao J, Xiao L, and Jia S 2022 *Chin. Phys. Lett.* **39** 013401

[45] Vacher M, Steinberg L, Jenkins A J, Bearpark M J, and Robb1 M A 2015 *Phys. Rev. A* **92** 040502(R)

[46] Despré V, Golubev N V, and Kuleff A I 2018 *Phys. Rev. Lett.* **121** 203002

[47] Yuan K J, Chelkowski S, and Bandrauk A D 2013 *J. Chem. Phys.* **138** 134316

[48] Yuan K J and Bandrauk A D 2016 *J. Chem. Phys.* **145** 194304

[49] Yuan K J and Bandrauk A D 2017 *Phys. Chem. Chem. Phys.* **19** 25846

[50] Yuan K J and Bandrauk A D 2019 *Appl. Sci.* **9** 1941

[51] Hermann G, Pohl V, Dixit G, and Tremblay J C 2020 *Phys. Rev. Lett.* **124** 013002

[52] Yu X, Zhang X, Hu X *et al.* 2022 *Phys. Rev. Lett.* **129** 023001

# Supporting Information: Quantum Engineering of Helical Charge Migration in HCCI

ChunMei Liu(刘春梅)[1], Jörn Manz(源满)[2,3,4*], Huihui Wang(王慧慧)[3,4], Yonggang Yang(杨勇刚)[3,4**]

[1] *Crystal Physics Research Center, College of Science, Nanjing University of Posts and Telecommunications, Nanjing 210023, China*

[2] *Institut für Chemie und Biochemie, Freie Universität Berlin, 14195 Berlin, Germany*

[3] *State Key Laboratory of Quantum Optics and Quantum Optics Devices, Institute of Laser Spectroscopy, Shanxi University, Taiyuan 030006, China;*

[4] *Collaborative Innovation Center of Extreme Optics, Shanxi University, Taiyuan 030006, China*

## I. Quantum chemical calculations of the electronic eigenfunctions, eigenenergies, the one-electron density matrix elements and the transition dipole matrix elements of the oriented HCCI

The electronic eigenfunctions $\Psi_j$ and eigenenergies $E_j$ of iodo acetylene HCCI oriented along the $z$-axis are calculated as solutions of the time-independent Schrödinger equation (TISE) $H_e\Psi_j = E_j\Psi_j$. The Hamiltonian $H_e$ accounts for the kinetic energy of the electrons, and for the Coulomb interactions of all electrons and the nuclei. The nuclear structure is frozen as shown in Fig. 1(a). It is adapted from Ref. [1] where it has been calculated by means of the coupled clusters singles doubles (triples)[2] method (CCSD(T)/cc-pVQZ*). Here cc-pVQZ* means Dunning's correlation consistent basis set with polarization functions for the valence electrons up to the quintuple-zeta level for all atoms.[3] The star indicates the use of proper pseudo-potentials and the corresponding pseudo-potential basis set ("cc-pVQZ-pp") for iodine.[4] We focus on just five eigenfunctions, namely $\Psi_0$ for the ground state with irreducible representation (IRREP) $\Sigma^+$, and the degenerate pairs $\Psi_{1x}, \Psi_{1y}$ and $\Psi_{2x}, \Psi_{2y}$ for the first and second excited $\Pi$ states. For convenience, the eigenfunctions are also denoted by their IRREPs, i.e. we set $\Psi_0 = 1\Sigma^+$, $\Psi_{1x} = 1\Pi_x$, $\Psi_{1y} = 1\Pi_{1y}$, $\Psi_{2x} = 2\Pi_x$, $\Psi_{2y} = 2\Pi_y$. They depend on the spatial ($\mathbf{r}_n$) and spin ($\alpha_n$ or $\beta_n$) coordinates of $N = 16$ valence electrons, $n = 1, 2, ..., N$. In short-hand notation, they are written as $\Psi_j(\mathbf{r}_1, \mathbf{r}_2, ..., \mathbf{r}_N)$, without explicit notation of the spins.

The TISE is solved by means of the state averaged complete active state self-consistent field method[5] (CASSCF(16,13)/cc-pVQZ*) for all atoms, as implemented in MOLPRO.[6] For convenience, these calculations assume $C_{2v}$ symmetry of HCCI. Subsequently, the resulting IRREPs of the wavefunctions are re-assigned to $C_{\infty v}$ symmetry, in particular $A_1 \to \Sigma^+$ for the ground state and $B_1 \to \Pi_x$, $B_2 \to \Pi_y$ for the degenerate excited $\Pi$ states.

Using the eigenfunctions $\Psi_j(\mathbf{r}_1, \mathbf{r}_2, ..., \mathbf{r}_N)$, we employ the ORBKIT package[7–9] to calculate the corresponding diagonal and off-diagonal matrix elements of the one-electron density,

$$\begin{aligned}\rho_{ij}(\mathbf{r}) &= \int ... \int \psi_i(\mathbf{r}_1, \mathbf{r}_2, ..., \mathbf{r}_N)\psi_j(\mathbf{r}_1, \mathbf{r}_2, ..., \mathbf{r}_N) \sum_{n=1}^{N} \delta(\mathbf{r} - \mathbf{r}_n) d\mathbf{r}_1 d\mathbf{r}_2 ... d\mathbf{r}_N \\ &= N \int ... \int \psi_i(\mathbf{r}, \mathbf{r}_2, ..., \mathbf{r}_N)\psi_j(\mathbf{r}, \mathbf{r}_2, ..., \mathbf{r}_N) d\mathbf{r}_2 d\mathbf{r}_3 ... d\mathbf{r}_N.\end{aligned} \tag{S1}$$

Using the $\rho_{ij}(\mathbf{r})$, the transition dipole matrix elements $\mathbf{d}_{ij}$ for the transitions between states $i$ and $j$ are calculated as

$$\mathbf{d}_{ij} = -e \cdot \int \mathbf{r}\rho_{ij}(\mathbf{r}) d\mathbf{r}. \tag{S2}$$

The corresponding permanent dipoles $\mathbf{d}_{jj}$ of the oriented HCCI in state $j$ are calculated by MOLPRO.

The resulting energy levels of the ground state $1\Sigma^+$ and the degenerate excited states $1\Pi_x, 1\Pi_y$ and $2\Pi_x, 2\Pi_y$ are 0.00 eV, 5.60 eV and 7.88 eV, respectively. The values of the non-zero components of the permanent dipoles

*Electronic address: (Yang Y) ygyang@sxu.edu.cn;(Manz J) jmanz@chemie.fu-berlin.de

and the transition dipole matrix elements for the symmetry allowed transitions between these states are

$$\begin{aligned}
&(d_z)_{00} = -0.0115ea_0, (d_z)_{1x,1x} = (d_z)_{1y,1y} = -0.9237ea_0, \\
&(d_z)_{2x,2x} = (d_z)_{2y,2y} = -1.6994ea_0, (d_x)_{0,1x} = (d_y)_{0,1y} = 0.3164ea_0, \\
&(d_x)_{0,2x} = (d_y)_{0,2y} = 0.1163ea_0, (d_z)_{1x,2x} = (d_z)_{1y,2y} = 1.2418ea_0.
\end{aligned} \tag{S3}$$

**II. Quantum simulations of the laser driven electron dynamics of the oriented HCCI**

The laser driven electron dynamics of the oriented HCCI is represented by the time-dependent electronic wavefunction $\Psi(t)$. It is calculated, in semiclassical dipole ($\hat{\mathbf{d}}$) approximation, as solution of the time-dependent Schrödinger equation (TDSE)

$$i\hbar\frac{\partial\Psi(t)}{\partial t} = H(t)\Psi(t) \tag{S4}$$

with Hamiltonian

$$\boldsymbol{H}(t) = \boldsymbol{H}_e - \hat{\mathbf{d}}\cdot\boldsymbol{\epsilon}(t) = \boldsymbol{H}_e - \hat{d}_x\epsilon_x(t) - \hat{d}_y\epsilon_y(t) - \hat{d}_z\epsilon_z(t), \tag{S5}$$

where $\boldsymbol{\epsilon}(t) = \boldsymbol{\epsilon}_{\rm I}(t)$ or $\boldsymbol{\epsilon}(t) = \boldsymbol{\epsilon}_{\rm II}(t)$ is the electric field of the laser pulses for strategy I or II, respectively, cf. eqns. (1), (2) of the main text. Note that $\boldsymbol{\epsilon}_{{\rm II},z}(t) = 0$ because strategy II uses circularly polarized laser pulses, exclusively. The TDSE (S4) is solved subject to the initial ($t = t_i = -5$ fs) condition

$$\Psi(t_i) = \Psi_0 \tag{S6}$$

representing the HCCI molecule in its electronic ground state. Subsequently, the laser pulses excite the molecule, partially to

$$\psi_1 = \frac{1}{\sqrt{2}}\left(\psi_{1x} + i\psi_{1y}\right), \psi_2 = \frac{1}{\sqrt{2}}\left(\psi_{2x} + i\psi_{2y}\right). \tag{S7}$$

The wavefunction is, therefore, written as

$$\Psi(t) = c_0(t)\Psi_0 + c_1(t)\Psi_1 + c_2(t)\Psi_2. \tag{S8}$$

In principle, one may include additional electronic eigenfunctions in the expansion (S8), but this is not necessary, for two reasons: First, according to our calculations there are only few additional eigenstates within the spectral widths ($= \hbar/2\tau$) of the transform-limited laser pulses but none of them has proper components of the transition dipoles as requested in Fig. 1 (For example, they may have non-zero $z$-components while non-zero $x, y$-components are needed, or vice versa.) Second, in view of the small populations of the excited states, we assume that ladder climbing to even more excited states is negligible. The restriction of the expansion (S8) to just three states implies that the corresponding probabilities of occupying states $j = 0, 1, 2$

$$P_j(t) = |c_j(t)|^2 \tag{S9}$$

are normalized,

$$\sum_{j=0}^{2} P_j(t) = 1. \tag{S10}$$

Using the Ansatz (S8), the TDSE (S4) can be rewritten as differential equation for the vector of the coefficients $\boldsymbol{c}(t) = (\boldsymbol{c}_0(t), \boldsymbol{c}_1(t), \boldsymbol{c}_2(t))^T$ (see e. g. Refs.[10,11])

$$i\hbar\frac{d\boldsymbol{c}(t)}{dt} = \boldsymbol{H}(t)\boldsymbol{c}(t). \tag{S11}$$

The nine matrix elements of the $3\times 3$ Hamilton matrix $\hat{\boldsymbol{H}}(t)$ are

$$H_{ij}(t) = H_{e,ij} - \boldsymbol{d}_{ij}\cdot\boldsymbol{\epsilon}(t), \tag{S12}$$

which consists of the diagonal term for the electronic energies,

$$H_{e,ij} = E_i\delta_{ij} \tag{S13}$$

and the terms for the laser-dipole couplings, cf. eqn. (S3).

The algebraic version of the TDSE (S11) is solved by means of the simple Euler method for the interaction picture, as in Ref.[10]. Converged results are obtained for the equidistant time step, $\Delta t = 0.001$ fs.

**III. Determination of the parameters of optimal laser pulses for quantum engineering of helical charge migration in oriented HCCI**

The TDSE (S4) and the algebraic version (S11) are valid for a large variety of laser pulses which induce helical charge migration (HCM) in the oriented HCCI, according to the strategies I or II. Here we present quantum engineering of HCM for an illuminating example which demonstrates the equivalence of the two different approaches. For this purpose, the laser pulses must be designed such that for both cases I and II, they drive the electronic wavefunction from the initial ground state (S6) to the same target state for HCM,

$$\Psi(t_f) = c_0(t_f)\Psi_0 + c_1(t_f)\Psi_1 + c_2(t_f)\Psi_2 \tag{S14}$$

at the end ($t = t_f = 5$fs) of the laser pulse. For the present example, the target coefficients are chosen rather arbitrarily to be real-valued,

$$c_j(t_f) \equiv C_j = \sqrt{P_j}(t_f) \tag{S15}$$

with probabilities

$$P_0(t_f) = 0.97, P_1(t_f) = 0.02, P_2(t_f) = 0.01. \tag{S16}$$

Subsequently, for times $t' = t - t_f > 0$, the electronic wavefunction

$$\Psi(t') = C_0\Psi_0 + C_1 e^{-iE_1 t'/\hbar}\Psi_1 + C_2 e^{-iE_2 t'/\hbar}\Psi_2 \tag{S17}$$

represents HCM, as shown in the main text, cf. Figs. 3.

The analytical form of the laser pulses is specified in the main text, cf. eqns. (1), (2). Here we present the method for determining the laser parameters $lp = \{\epsilon, \tau, \omega, \eta\}$ of the individual pulses such that they yield the same HCM (S17) by means of strategies I and II. It has four steps:

(i) We use resonant frequencies such that

$$\hbar\omega_{ij} = E_j - E_i. \tag{S18}$$

(ii) The durations of the pulses are set equal to a rather small value, to support the present scenario of frozen nuclei.[1,10]

$$\tau_{01} = \tau_{12} = \tau_{02} \equiv \tau = 2.5fs. \tag{S19}$$

(iii) Next, the amplitudes of the electric fields are determined such that the laser pulses yield the same target probabilities (S16) for both strategies I and II. In principle, this can be achieved by means of brute force scans of the amplitudes versus the resulting probabilities. Alternatively, we use an illuminating two (sub-)step approach. The first sub-step determines reasonable approximations. The second sub-step starts from the approximations and determines neighboring values for perfect quantum control, by systematic fine-tuning.

Specifically, the first sub-step makes use of the fact that strategies I and II employ superpositions of two laser pulses which should induce specific transitions between two electronic eigenstates of the oriented HCCI. The literature has simple rules for the field strength of laser pulses with Gaussian envelopes which achieve the target transitions between two states.[10,12] These rules have been derived by means of the rotating wave approximation, and they are employed here as zero-order approximations for our purposes. For example, for strategy I, the right (+) circularly polarized laser pulse should transfer about 0.03 population from $\Psi_0$ to $\Psi_1$. For this purpose, the approximate value of the field amplitude $\epsilon_{01,I}$ should satisfy the condition $\sin^2(\sqrt{\pi}\epsilon_{01,I}(d_x)_{0,1x}\tau_{01}/\sqrt{2}\hbar) = 0.03$.[10] The linearly $z$-polarized laser pulse of strategy I should transfer 1/3 of the population from $\Psi_1$ to $\Psi_2$. Accordingly, the approximate value of the field amplitude $\epsilon_{12,I}$ should satisfy the condition[10,12] $\sin^2(\sqrt{\pi}\epsilon_{12,I}(d_z)_{1x,2x}\tau_{12}/2\hbar) = 1/3$. Likewise, for strategy II, the two right (+) circularly polarized pulses should transfer $P_1(t_f) = 0.02$ and $P_2(t_f) = 0.01$ populations from $\Psi_0$ to $\Psi_1$ and from $\Psi_0$ to $\Psi_2$; for these purposes, the corresponding field strengths should satisfy the conditions $\sin^2(\sqrt{\pi}\epsilon_{01,II}(d_x)_{0,1x}\tau_{01}/\sqrt{2}\hbar) = 0.02$ and $\sin^2(\sqrt{\pi}\epsilon_{02,II}(d_x)_{0,2x}\tau_{02}/\sqrt{2}\hbar) = 0.01$, respectively.[10] Starting from the approximate values $\epsilon_{01,I}, \epsilon_{12,I}$ and $\epsilon_{01,II}, \epsilon_{02,II}$, the second sub-step then yields close-lying values $\epsilon_{01,I}$ for

perfect quantum control of the target populations. The values of the target field strengths are listed in Table SI-1.

(iv) Finally, the carrier envelope phases (CEP) are determined such that they yield the real-valued coefficients (S15). Again, in principle, this can be achieved by means of brute force scans of the CEPs versus the resulting phases of the coefficients. Alternatively, we use an efficient two (sub-)step approach. Specifically for strategy I, we vary $\eta_{01}$ in the domain $[0, 2\pi]$ till we obtain the same phases for the coefficients $c_0(t_f)$ and $c_1(t_f)$. Subsequently, we vary $\eta_{12}$ till we obtain the same phases for the coefficients $c_1(t_f)$ and $c_2(t_f)$. This way, we arrive at coefficients $c_0(t_f), c_1(t_f), c_2(t_f)$ which possess the same (irrelevant) global phase; the latter can be re-set to zero, such that the coefficients are real-valued and positive.

Likewise for strategy II, we vary $\eta_{01}$ and $\eta_{02}$ independently till we obtain the same phase for all coefficients $c_0(t_f), c_1(t_f)$ and $c_2(t_f)$. This global phase is then set equal to zero, i.e. the coefficients are real-valued and positive. The resulting CEPs for perfect quantum control by equivalent strategies I and II are also listed in Table SI-1.

Table SI- 1: Laser parameters $lp = \{\epsilon, \tau, \omega, \eta\}$ for quantum engineering of helical charge migration in oriented HCCI[a]

| Strategy | target $\rightarrow$ transition[b] | polarization[c] | $\epsilon$/(GV/m) | $\tau$/fs | $\hbar\omega$/eV[d] | T/fs[e] | $\eta$ |
|---|---|---|---|---|---|---|---|
| I | $\Psi_0 \rightarrow \Psi_1$ | circular | 2.345 | 2.5 | 5.60 | 0.74 | $\pi - 0.103$ |
| I | $\Psi_1 \rightarrow \Psi_2$ | linear | 5.578 | 2.5 | 2.28 | 1.81 | $\pi + 0.002$ |
| II | $\Psi_0 \rightarrow \Psi_1$ | circular | 1.792 | 2.5 | 5.60 | 0.74 | $\pi - 0.101$ |
| II | $\Psi_0 \rightarrow \Psi_2$ | circular | 3.446 | 2.5 | 7.88 | 0.53 | $\pi + 1.420$ |

[a] cf. eqns. (1),(2) in main text. The corresponding maximum intensities of the laser pulses for strategies I and II are 9.725 and 4.007 TW/cm$^2$, respectively. $\epsilon$ =field amplitude, $\tau$ =duration, $\omega$ =carrier frequency, $\eta$ =carrier envelope phase CEP.

[b] $\Psi_0 = 1\Sigma^+, \Psi_1 = (1\Pi_x + i \cdot 1\Pi_y)/\sqrt{2}, \Psi_2 = (2\Pi_x + i \cdot 2\Pi_y)/\sqrt{2}$.

[c] circular = right (+) circularly polarized, linear = linearly $z$-polarized.

[d] resonant photon energy, $\hbar\omega_{ij} = E_j - E_i$.

[e] period $T_{ij} = 2\pi/\omega_{ij}$.

## IV. Time-dependent one-electron density matrices and dipoles documenting helical charge migration in HCCI after the laser control

The electronic wavefunction (S17) represents helical charge migration in the oriented HCCI for the time after the laser pulse, $t' = t - t_f > 0$. This is illustrated in Figs. 3 and SI-1 by the time-dependent dipole $\hat{\mathbf{d}}(t')$ and by snapshots of the one-electron density difference $\Delta\rho(t')$, respectively. This Section explains the methods for calculating $\Delta\rho(t')$ and $\hat{\mathbf{d}}(t')$.

The wavefunction (S17) yields the time-dependent N-electron density

$$
\begin{aligned}
\tilde{\rho}(t') &= \psi(t')\psi^*(t') \\
&= C_0^2\psi_0\psi_0^* + C_1^2\psi_1\psi_1^* + C_2^2\psi_2\psi_2^* + C_0C_1\left(\psi_0\psi_1^* e^{i\omega_{01}t'} + \psi_0^*\psi_1 e^{-i\omega_{01}t'}\right) \\
&+ C_0C_2\left(\psi_0\psi_2^* e^{i\omega_{02}t'} + \psi_0^*\psi_2 e^{-i\omega_{02}t'}\right) + C_1C_2\left(\psi_1\psi_2^* e^{i\omega_{21}t'} + \psi_1^*\psi_2 e^{-i\omega_{21}t'}\right) \\
&= C_0^2\psi_0^2 + \frac{C_1^2}{2}\left(\psi_{1x}^2 + \psi_{1y}^2\right) + \frac{C_2^2}{2}\left(\psi_{2x}^2 + \psi_{2y}^2\right) + \sqrt{2}C_0C_1[\psi_0\psi_{1x}\cos(\omega_{01}t') + \psi_0\psi_{1y}\sin(\omega_{01}t')] \\
&+ \sqrt{2}C_0C_2\left[\psi_0\psi_{2x}\cos(\omega_{02}t') + \psi_0\psi_{2y}\sin(\omega_{02}t')\right] \\
&+ C_1C_2\left[(\psi_{1x}\psi_{2x} + \psi_{1y}\psi_{2y})\cos(\omega_{21}t') + (\psi_{1x}\psi_{2y} - \psi_{1y}\psi_{2x})\sin(\omega_{21}t')\right].
\end{aligned}
\tag{S20}
$$

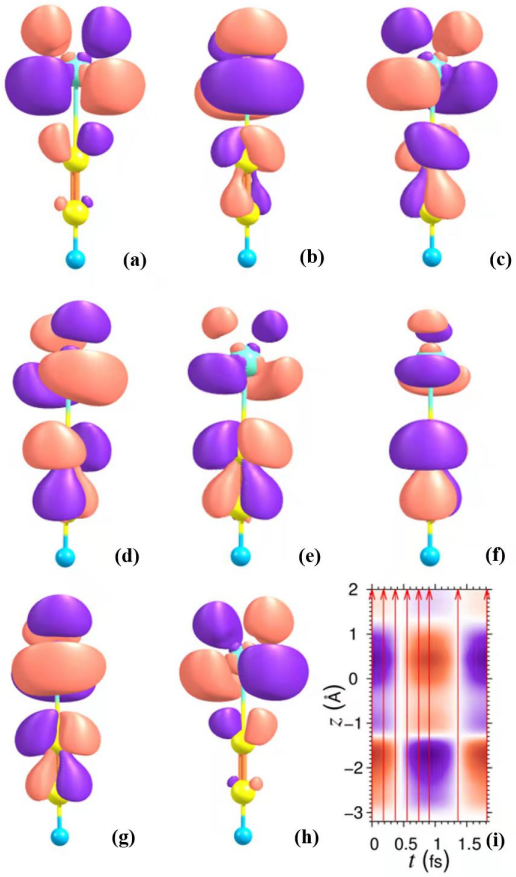


**Fig. SI-1.** Helical charge migration (HCM) of HCCI oriented along the laboratory $z$-axis, for times $t' = t - t_f > 0$ after the end ($t_f = 5$ fs) of the laser pulses for strategy I (cf. Figs. 1(c) and 2) or for strategy II (cf. Figs. 1(c) and 4). (a)-(h) Snapshots of the one-electron density difference $\Delta\rho(t') = \rho(t') - \bar{\rho}$ between the density at $t'$ and the mean density. Domains with enhanced ($\Delta\rho(t') > 0$) and with diminished ($\Delta\rho(t') < 0$) densities are represented by orange- and purple-colored lobes, respectively. HCCI oriented along the $z$-axis is illustrated by a stick-and-ball cartoon, cf. Fig. 1(a). The scaling is the same in all panels (a)-(i), with the center-of-mass at $z = 0$. The snapshots (a)-(e) are at times $t' = k \cdot T_{01}/4, k = 0, 1, .., 4$ with $T_{01} = h/(E_1 - E_0) = 0.74$ fs. They illustrate the circular charge migration (CCM) as component of HCM. Snapshots (a), (f), (g), (h) are at times $t' = k \cdot T_{12}/4, k = 0, 2, 3, 4$ with $T_{12} = h/(E_2 - E_1) = 1.81$ fs, during linear charge migration (LCM), the other building-stone of HCM. (i) The LCM component of HCM is documented by the contour plot of $\Delta\rho_z(z, t') = \int\int dxdy\Delta\rho(x, y, z, t')$. The sequence of eight vertical arrows marks the times for the snapshots (a)-(h).

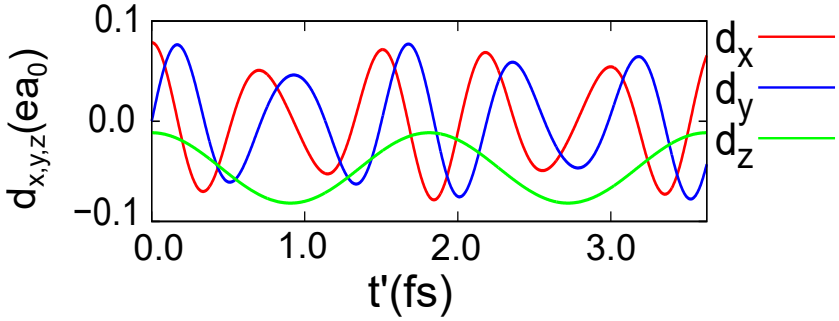


**Fig. SI-2.** The components $d_x(t'), d_y(t'), d_z(t')$ of the helical dipole $\mathbf{d}(t')$ shown in Fig.3. The $x-$ and $y-$ components document quasi-periodic CCM with the quasi-periodic circular charge migration (CCM) component of HCM, with $T_{01} = 0.74$ fs. The $z$-component documents periodic linear charge migration (LCM) component of HCM, with period $T_{12} = 1.81$ fs.

This in turn yields the time-dependent one-electron density

$$\begin{aligned}\rho(\mathbf{r},t') &= \int ... \int \tilde{\rho}(\mathbf{r}_1,\mathbf{r}_2,...,\mathbf{r}_N,t') \sum_{n=1}^{N} \delta(\mathbf{r}-\mathbf{r}_i) d\mathbf{r}_1 d\mathbf{r}_2 ... d\mathbf{r}_N \\ &= N \int ... \int \tilde{\rho}(\mathbf{r},\mathbf{r}_2,...,\mathbf{r}_N,t) d\mathbf{r}_2 d\mathbf{r}_3 ... d\mathbf{r}_N \\ &= C_0^2\rho_{00} + \frac{C_1^2}{2}(\rho_{1x,1x}+\rho_{1y,1y}) + \frac{C_2^2}{2}(\rho_{2x,2x}+\rho_{2y,2y}) \\ &+ \sqrt{2}C_0C_1\left[\rho_{0,1x}\cos(\omega_{01}t') + \rho_{0,1y}\sin(\omega_{01}t')\right] \\ &+ \sqrt{2}C_0C_2\left[\rho_{0,2x}\cos(\omega_{02}t') + \rho_{0,2y}\sin(\omega_{02}t')\right] \\ &+ C_1C_2\left[(\rho_{1x,2x}+\rho_{1y,2y})\cos(\omega_{21}t') + (\rho_{1x,2y}-\rho_{1y,2x})\sin(\omega_{21}t')\right].\end{aligned} \tag{S21}$$

The time-averaged mean value of $\rho(\mathbf{r},t')$ is

$$\bar{\rho}(\mathbf{r}) = C_0^2\rho_{00} + \frac{C_1^2}{2}\left(\rho_{1x,1x}+\rho_{1y,1y}\right) + \frac{C_2^2}{2}\left(\rho_{2x,2x}+\rho_{2y,2y}\right). \tag{S22}$$

From eqns. (S23) and (S24) we obtain the time-dependent density difference

$$\Delta\rho(\mathbf{r},t') = \rho(\mathbf{r},t') - \bar{\rho}(\mathbf{r}) \tag{S23}$$

documented by snapshots in Fig. SI-1.

Contour plots SI-1(a) - SI-1(e) of $\Delta\rho(t')$ illustrate the CCM component of HCM around the molecular axis. Contour plots SI-1(a), SI-1(f) - SI-1(h) are taken during LCM from the C-I bond to the C=C bond, and back. The contour plot of $\Delta\rho_z(z,t') = \int\int dxdy\Delta\rho(x,y,z,t')$ in panel 3(i) documents LCM quantitatively, as in Refs. [10,13].

Finally, the time-dependent dipole moment is calculated using the time-dependent one-electron density $\rho(\mathbf{r},t')$ and the time-independent charge density $\rho_c(\mathbf{r})$ of the system formed by all the nuclei and all the core electrons,

$$\begin{aligned}\mathbf{d}(t') &= -e\cdot\int \mathbf{r}\rho(\mathbf{r},t')d\mathbf{r} + \int \mathbf{r}\rho_c(\mathbf{r})d\mathbf{r} = C_0^2\mathbf{d}_{00} + \frac{C_1^2}{2}\left(\mathbf{d}_{1x,1x}+\mathbf{d}_{1y,1y}\right) + \frac{C_2^2}{2}\left(\mathbf{d}_{2x,2x}+\mathbf{d}_{2y,2y}\right) \\ &+ \sqrt{2}C_0C_1\left[\mathbf{d}_{0,1x}\cos(\omega_{01}t') + \mathbf{d}_{0,1y}\sin(\omega_{01}t')\right] \\ &+ \sqrt{2}C_0C_2\left[\mathbf{d}_{0,2x}\cos(\omega_{02}t') + \mathbf{d}_{0,2y}\sin(\omega_{02}t')\right] \\ &+ C_1C_2\left[(\mathbf{d}_{1x,2x}+\mathbf{d}_{1y,2y})\cos(\omega_{21}t') + (\mathbf{d}_{1x,2y}-\mathbf{d}_{1y,2x})\sin(\omega_{21}t')\right].\end{aligned} \tag{S24}$$

Using eqn. (S3), (S15), (S16), this yields the time evolution of the Cartesian components of the dipole, as illustrated in Fig. SI-2.

$$\begin{aligned}d_x(t')/ea_0 &= 0.0623\cos(\omega_{01}t') + 0.0162\cos(\omega_{02}t') \\ d_y(t')/ea_0 &= 0.0623\sin(\omega_{01}t') + 0.0162\sin(\omega_{02}t') \\ d_z(t')/ea_0 &= -0.0466 + 0.0351\cos(\omega_{21}t').\end{aligned} \tag{S25}$$

The corresponding helical path of $\mathbf{d}(t')$ is shown in Fig. 3, mapping helical charge migration in the oriented HCCI.

**V. On the equivalence of the strategies I and II for quantum engineering of helical charge migration in oriented HCCI**

The equivalence of the quantum strategies I and II rests on the fact that they yield the same wavefunction (3), for times $t' = t - t_f > 0$. This is because they yield the same coefficients $c_j(t_f)$ at the end of the laser pulses. The subsequent coherent quantum dynamics proceeds without any memory - it does not depend on the strategies for preparing the $c_j(t_f)$. Specifically, strategy I transfers population from the ground state $j = 0$

to the two excited states $j = 1$ and 2, by laser-induced transitions $0 \rightarrow 1$ and $1 \rightarrow 2$. In contrast, strategy II achieves the same effect by transitions $0 \rightarrow 1$ and $0 \rightarrow 2$. The symmetry selection rules for the transitions require that the linearly polarized pulse for $1 \rightarrow 2$ (strategy I) has to be substituted by the circularly polarized pulse for $0 \rightarrow 2$ (strategy II).

# References


[1] Kraus P M, Mignolet B, Baykusheva D, Rupenyan A, Horný L, et al. 2015 *Science* **350** 790-795.
[2] Deegan M J O and Knowles P J 1994 *Chem. Phys. Lett.* **227** 321-326.
[3] Dunning Jr. T H 1989 *J. Chem. Phys.* **90** 1007.
[4] Peterson K A, Shepler B C, Figgen D and Stoll H 2006 *J. Phys. Chem. A* **110** 13877.
[5] Knowles P J and Wörner H-J 1985 *Chem. Phys. Lett.* **115** 259.
[6] Wörner H-J, et al. MOLPRO, version 2012.1, A package of ab initio programs. http://www.molpro.net, 2012.
[7] Hermann G, Pohl V, Tremblay J C, Paulus B, Hege H -C and Schild A 2016 *J. Comput. Chem.* **37** 1511-1520.
[8] Hermann G, Pohl V and Tremblay J C 2017 *J. Comput. Chem.* **38** 2378-2387.
[9] Pohl V, Hermann G and Tremblay J C 2017 *J. Comput. Chem.* **38** 1515-1527.
[10] Jia D, Manz J and Yang Y 2017 *J. Mod. Opt.* **64** 960.
[11] Barth I and Manz J 2006 *Angew. Chem. Int. Ed.* **45** 2962-2965.
[12] Liu C, Manz J and Yang Y 2015 *ChemPhysChem* **16** 191.
[13] Jia D, Manz J and Yang Y 2019 *J. Phys. Chem. Lett.* **10** 4273.